IEEE Access
Multidisciplinary | Rapid Review | Open Access Journal

Received 5 August 2025, accepted 21 August 2025, date of publication 29 August 2025, date of current version 12 September 2025.

Digital Object Identifier 10.1109/ACCESS.2025.3603726

RESEARCH ARTICLE

Modeling and Classifying Parkinsonian Tremors With Nonlinear Dynamics and Kalman Optimization

V. VANITHA[1], V. DHILIP KUMAR[2], OANA GEMAN[3,4], (Senior Member, IEEE), OCTAVIAN POSTOLACHE[5,6], (Senior Member, IEEE), SRI KRISHNA BELLAM[1], AND ROXANA TODEREAN[7], (Member, IEEE)

[1]Department of Artificial Intelligence and Machine Learning, Sri Ramachandra Faculty of Engineering and Technology, Chennai 600116, India
[2]Computer Science and Engineering, Vel Tech Rangarajan Dr. Sagunthala Research and Development Institute of Science and Technology, Chennai 600062, India
[3]Data Science and AI, Computer Science and Engineering, Chalmers University of Technology, 412 96 Gothenburg, Sweden
[4]University of Gothenburg, 405 30 Gothenburg, Sweden
[5]Instituto de Telecomunicações, 3810-193 Aveiro, Portugal
[6]ISCTE-Instituto Universitário de Lisboa, 1649-026 Lisbon, Portugal
[7]Department of Computers, Electronics and Automation, Ştefan cel Mare University of Suceava, 720229 Suceava, Romania

Corresponding author: Roxana Toderean (roxana.toderean@usm.ro)

ABSTRACT Parkinson Disease (PD) is a chronic neurodegenerative disorder due to the degeneration of dopamine-producing neurons in a brain region, crucial for motor function regulation. Rest tremor is a vital parameter and is essential to diagnose the disease and assess its prognosis. The frequency of rest tremor is a key characteristic to differentiate it from other types of tremors such as Essential tremors. This highlights the need for reliable and accurate methods to estimate the rest tremor frequency as accurate as possible. This paper proposes a novel method, Extended Lagrangian combined with Kalman techniques for rest tremor frequency extraction. The Extended Lagrangian mechanism addresses the irregular oscillatory behavior of rest tremor by incorporating energy dissipation via Rayleigh's dissipation function, nonlinear stiffness, as well as external forces. This mechanism serves as a foundation and helps to track the oscillatory nature of tremors. The video recordings of PD tremor taken in clinical settings may contain noise and have significant impact on the rest frequency estimate. The proposed approach addresses this issue, thus improving the accuracy of these estimates. This algorithm is validated on a dataset of 60 video recordings from PD patients, annotated by movement disorder specialists. The rest tremor frequency, along with other key features are then passed to a classifier to determine the severity of PD. The model achieved an accuracy of 98% with 1D CNN-LSTM classifier. This approach could be used in remote health assessment for PD patients, providing increased convenience to patients and caregivers.

INDEX TERMS Deep learning, Kalman filter, Lagrangian mechanism, Parkinson disease, rest tremor.

I. INTRODUCTION

Parkinson Disease (PD) is a nervous condition due to the loss of dopamine-generating neurons. As these neurons deteriorate, patients experience motor-related symptoms like uncontrollable shaking (rest tremors), muscle rigidity, slowed physical actions, and, over time, difficulty in maintaining balance. Non-motor issues, including emotional imbalances and disturbed sleep, also develop as PD advances. PD affects older adults, with nearly 1% of the global population over 60 years of age being affected. The rise in life expectancy and aging societies are predicted to escalate PD cases worldwide [1]. In India, a surge in PD cases is driven not only by these global patterns, but also by factors like urban expansion, dietary changes, and environmental triggers such as toxin exposure [2]. Mortality related to PD has

The associate editor coordinating the review of this manuscript and approving it for publication was Bing Li.

increased significantly, by 87.9% at an average annual rate of 3.8%.

Parkinson research and clinical practice emphasize evaluating rest tremor patterns as a key indicator for early-stage detection. The frequency patterns of rest tremor provide essential information about the status or advancement of the disease [3]. Standard diagnostics techniques based on neurologist observations and evaluations form the basis of current diagnostic practice. Such assessments based on subjective evaluation require additional objective measurement methods due to inter-rater variability.

The integration of Artificial Intelligence (AI) techniques for detecting tremors offers several advantages over sensors and other related approaches. Firstly, it enables straightforward assessments via video recording. This approach would be very valuable for Parkinson patients in geographically isolated or resource-limited settings. Secondly, these models can be used to analyze very large datasets reliably and identify even small variations of tremors that remain inconspicuous to the human observer. This enables earlier diagnosis of PD, before the clinical symptoms appear. Despite the promising advances in video based PD severity classification methods, many challenges remain to be addressed. A major challenge is developing robust models to distinguish PD tremor from tremors of other movement disorder, especially at the early stage. PD-related tremors could resemble other non-Parkinsonian tremors, such as essential tremor or tremor induced by drug side effects. The characteristics of the PD tremor vary from one patient to another, depending on the affected part of the body, patient's age, health, medications, and progression of the disease. Furthermore, cultural or genetic differences can influence the presentation and manifestation of the disease [4]. Additional challenges arise when transitioning from controlled environments to real-world clinical settings. Clinical environments have varying lighting conditions, equipment, and human movements that impact the quality of video recording. To address these issues, this study presents two new approaches: (i) a framework to detect rest tremor frequency in noisy environments (ii) an automated tool to capture and quantify Parkinson tremor severity based on rest tremor frequency and other significant features.

The contributions of this study are:

Adaptive Nyquist-Compliant Sparse Sampling (ANCSS) for PD Tremor Video Analysis: Adaptive Nyquist-Compliant Sparse Sampling (ANCSS) first detects tremor onset in video and discards preonset frames. It then analyzes a short segment using FFT to estimate the dominant tremor frequency, dynamically setting a Nyquist-compliant sampling rate. The proposed approach reduces computational overhead and makes it suitable for resource-limited settings.

Extended Lagrangian Mechanics for Rest Tremor Modeling: This framework extends classical Lagrangian mechanics by incorporating energy dissipation (Rayleigh's dissipation function), nonlinear stiffness, and external forces, specifically tailored to capture the irregular oscillatory nature of rest tremors, which traditional models do not fully address.

Nonlinear Stiffness and Damping for Frequency Shift Adaptation: Unlike conventional tremor models that assume periodic oscillations, this research accounts for tremor non-periodicity by incorporating nonlinear stiffness and damping factors, allowing the framework to adapt to real-world variations in tremor frequency due to fatigue, voluntary movements, and other patient-specific factors.

II. LITERATURE REVIEW

Recently, diverse methods including wearable sensors, video analysis, signal processing and deep learning have been applied to classify Parkinson's disease severity. This synthesis of studies from 2019 to 2024 highlights advancements in early detection and symptom quantification. The utilization of sensor model was promising and has great potential. [5] reviewed the digital biomarkers after evaluating the data obtained from the wrist-worn sensors concerning the PD symptoms in a group of 343 PD patients and 157 healthy controls. Similarly, [6] created a real-time smartwatch algorithm for PD detection, achieving results strongly aligned with clinical metrics. In a study [7],it is further validated that smartwatch based approach to assess motor symptom for 45 PD patients, closely matched clinical observations. A review by [8] confirmed that smartphone-based assessments of gait, balance, and dexterity are sufficiently robust for clinical integration.

Video analysis has also emerged as a powerful tool. Reference [9] achieved a 91.5% accuracy rate in distinguishing PD patients from healthy controls through gait analysis. Reference [10] applied pose-estimation techniques to evaluate motor symptoms in 150 PD patients, showing significant clinical relevance. Other notable contributions include the work of [11], who developed a system to detect PD from facial expressions with 95% accuracy. A study [12] on Leap Motion-based hand movement classification (with 89% accuracy) further expanded non-invasive diagnostic options. Reference [13] differentiated PD cases from healthy individuals, while [14] focused on distinguishing tremor from non-tremor episodes. Reference [15] addressed tremor severity classification, enhancing accuracy in symptom prediction. Some studies adopted broader frameworks. Authors [16] conducted a dual analysis: first identifying PD versus non-PD cases, then categorizing tremor subtypes (e.g., Rest Tremor, Essential Tremor).

A study [17] introduced an automated framework for detecting PD from videos using deep learning. The proposed method examines 1,380 videos of motor tasks through segmentation methods that separate movements and motion magnification that amplifies even slight movements and frequency domain analysis. The model demonstrates an accuracy of 91.8% indicating its potential for real-time detection of Parkinson's disease through webcam analysis. In a pilot study with 70 videos, [18] proposed a method that achieved an accuracy of 79% for detecting bradykinesia. The method demonstrated a diagnosis accuracy of 63%

for detecting Parkinson's disease. The detection results are encouraging even though the research data is limited. Such initiatives highlight the possibilities of integrated strategies to enhance the accuracy of diagnosis.

Combining data through multimodal approaches has shown significant promise. Reference [19] combined accelerometer data with video analysis, to achieve better accuracy in severity classification. Reference [20] used wearable sensors and smartphone data to classify patients' severity levels of PD with 93% accuracy. Reference [21] has shown the opportunities of using edge computing in health care, including the real time analysis of Parkinson's disease symptoms from gait abnormalities. Reference [22], the research examines tremor, speech, and gait signals by applying non-linear dynamics tools in order to highlight their significance in the diagnosis of Parkinson's. Furthermore, the study also suggests a knowledge-based system for diagnosis, which utilizes non-linear features to facilitate early detection and personalized monitoring of Parkinson's disease. Reference [23] integrated the explainable AI models with deep learning models to generate meaningful clinical insights. Reference [24] established a predictive model based on Response Surface Methodology that optimizes Deep Brain Stimulation treatment parameters for Parkinson's disease tremor. By processing tremor signals using statistical and nonlinear tools, the model assists in personalizing DBS settings for better therapeutic response.

A study on VR applications in PD by [25] used motion capture for realistic symptom assessment and was tested on 50 PD patients. Reference [26] gathered recent developments in digital biomarkers, which also stressed the need for clinical effectiveness to ensure usefulness in real-world healthcare settings. These works demonstrate great advances in PD severity classification through the use of multiple modalities, such as wearable sensor integration with video analysis, interpretable AI models with clinically meaningful outcomes.

III. MATERIALS AND METHODS

The importance of rest tremor as a primary symptom is highlighted at the beginning of the section, followed by a description of the dataset. In the subsequent parts, the methodology for detecting the rest tremor frequency using the proposed framework is discussed in detail, a brief discussion on the extraction of other significant features of rest tremor is provided.

A. REST TREMOR IN PARKINSON

PD is estimated to affect over 6 million people globally. As it progresses, approximately 70% of the patients develop rest tremors, which are a key characteristic of Parkinsonism [27]. Tremor assessment is one of the motor symptoms included in the Unified Parkinson's Disease Rating Scale (UPDRS), and this research follows the guidelines provided by this scale. The main clinical characteristics of rest tremor in PD are:

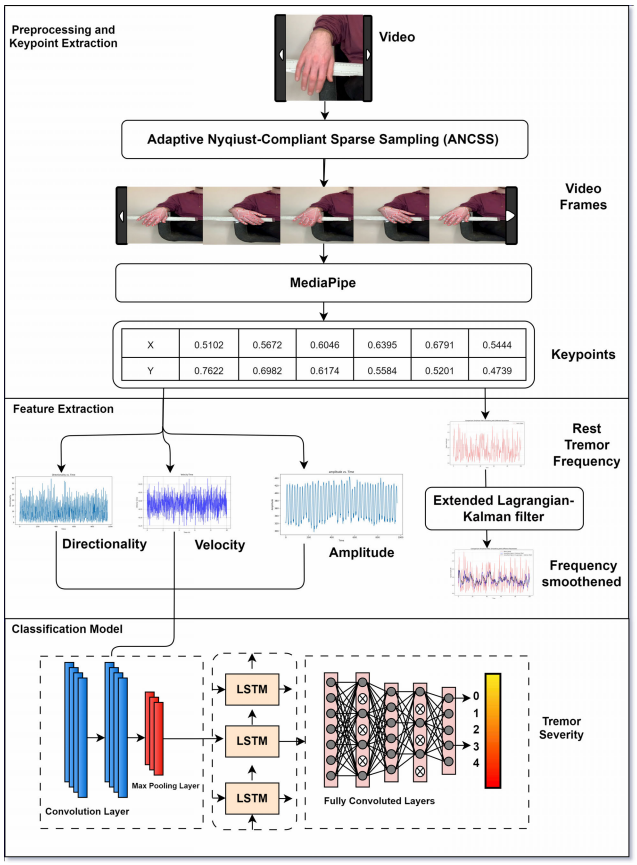

FIGURE 1. Workflow for parkinson severity classification from rest Tremor.

1) Frequency: PD tremors have a frequency of 4 to 6 Hz. Tremors can be associated with various neurological disorders but PD tremors have a distinct frequency [28].
2) Onset Pattern: Tremors are contracted asymmetrically initially; they often initiate in the hand or fingers; tremor can be described as pill-rolling due to the back-and-forth motion between the thumb and the index finger [29].
3) Progression:Over time, the tremors may extend to the ipsilateral limb, and later to the opposite side due to the progression of neurodegeneration [30].

B. METHOD

Figure 1 depicts the workflow for Parkinson severity classification using the proposed Extended Lagrangian-kalman (ELK) method. The dataset consists of recordings of Parkinson patients with varying severity levels and normal patients. The process begins with the ANCSS method to select informative frames from raw recording data. The frames are cropped to keep the hand as the main focus. In the second stage, 21 key points of the hand are then extracted from those cropped recordings using a pose estimation algorithm. The key features are extracted from these estimated key points, which are then passed to several classifiers to detect the severity of PD.

1) ADAPTIVE NYQUIST-COMPLIANT SPARSE SAMPLING (ANCSS)

PD tremors, particularly rest tremors, are rhythmic oscillations with a frequency range of 4-6 Hz, as established by prior studies [31], [32]. Video-based analysis requires sampling that adheres to the Nyquist-Shannon theorem (sampling frequency $> 2\times$ maximum signal frequency) to avoid aliasing and ensure accurate frequency estimation. However, processing every frame of a high-frame-rate video (e.g., 30 fps) is computationally expensive, especially for continuous, subtle motions like tremors. The methods of sparse or dense sampling from general video classification are not suitable for PD tremors as they either ignore fine temporal details or provide the algorithm with abundant unimportant data. ANCSS is proposed for efficient and accurate sampling of tremor data.

a: ANCSS PARAMETER SELECTION

Onset-Detection Threshold: The threshold values for tremor onset detection in the ANCSS framework were determined through systematic empirical analysis rather than arbitrary selection. Using a training subset of 20 videos spanning all severity classes, we evaluated pixel-wise difference thresholds ranging from 0.1 to 2.0 in increments of 0.1. The optimal threshold of 1.2 was selected based on maximizing the F1-score for onset detection when validated against manual expert annotations of tremor initiation timing. This threshold achieved 94.2% sensitivity and 91.7% specificity for onset detection, with a mean temporal error of 0.3 ± 0.8 seconds compared to expert-identified onset times

Frame Rate Selection Rationale: We chose a baseline sampling rate of 15 Hz based on Nyquist requirements for Parkinson's tremor (4–6 Hz), which corresponds to a $2.5\times$ safety margin over the maximum expected frequency. This conservative rate ensures adequate temporal resolution while minimizing computational overhead. Tremor-specific sampling rates are then dynamically computed as given in equation (1).

b: STEP 1: INITIAL FRAME RATE ASSESSMENT

The recording rate of 30 fps is beyond the Nyquist rate (14 Hz for PD tremors $\leq$ 7Hz) which implies that the dynamics of tremors are well captured without interference. This sets a solid basis for further adaptive subsampling (for instance, 15-9 fps with ANCSS), which maintains Nyquist compliance when determining tremor frequency but reduces computations. The high initial sampling rate can capture the worst-case tremor frequencies and retains frequency information while making fine adjustments.

c: STEP 2: TREMOR ONSET DETECTION

Since PD tremors typically emerge after a short delay (e.g., around 3 seconds when the patient stabilizes), frames captured before this onset are discarded to reduce the data volume. The tremor onset is detected through frame analysis and a threshold approach. The onset is determined by analysing the frames and computing the absolute pixel-wise difference between consecutive frames. When the pixel difference exceeds a threshold value, that frame is marked as the onset frame. All frames prior to this are discarded to minimize computational time.

d: STEP 3: ADAPTIVE SAMPLING RATE CALCULATION

Set the maximum tremor frequency ($f_{\max}$) to 7 Hz. The minimum required sampling frequency is greater than 14 Hz; hence, a baseline rate of 15 Hz is chosen. From the 30 fps video, sampling every second frame following the onset frame achieves an effective rate of 15 fps.

e: STEP 4: DYNAMIC ADJUSTMENT BASED ON TREMOR VARIABILITY

A 5-second segment after tremor onset is analyzed using FFT to estimate the dominant tremor frequency (f_{dom}). If $f_{\text{dom}} < 5$ Hz, the sampling rate is adjusted to

$$FPS' = 2 \times f_{\text{dom}} + \epsilon, \tag{1}$$

with $\epsilon = 1$ Hz; for example, if $f_{\text{dom}} = 4$ Hz then $\text{FPS}' = 9$ Hz (implying sampling every third frame). If $f_{\text{dom}} \geq 5$ Hz, FPS' is maintained at 15 Hz.

f: STEP 5: FRAME SELECTION AND PROCESSING

Frames are uniformly sampled from the tremor-active segment at the calculated interval (e.g., every second or third frame, depending on the determined FPS'), and these frames are passed to the tremor analysis pipeline which includes keypoint extraction, frequency estimation, and classification).

2) KEY POINT EXTRACTION

MediaPipe [33] is a framework for building multimodal applied machine learning pipelines, including pose estimation and hand tracking. In this stage, 21 landmarks on the hand corresponding to anatomical key points such as fingertips, joints, and wrist are detected using MediaPipe. These landmarks are identified as follows: 4 for each finger (tip, DIP, PIP, MCP joints) and 1 for the wrist. This level of detail is essential to ensure precise tracking of hand movements, enabling the analysis of very fine tremors that are characteristic of PD.

3) FEATURE EXTRACTION

After extracting the 21 landmarks from the input video dataset, the following key features are computed.

Rest Tremor Frequency: The rate of tremor oscillations per second, typically measured in hertz (Hz) In PD, this frequency lies in the range of 4-6 Hz.

Rest Tremor Amplitude: The extent or magnitude of hand or limb movements, corresponding to the severity of tremor. Higher amplitude corresponds to increased severity of the tremor.

Algorithm 1 Adaptive Nyquist-Compliant Sparse Sampling (ANCSS)

INITIALIZE(V, FPS_{orig}, f_{max}, ϵ, T_{seg}, $Pipeline$)
  $N_{total} \leftarrow$ length(V)
  $T_{total} \leftarrow N_{total}/FPS_{orig}$
  assert $FPS_{orig} > 2 \times f_{max}$
  $onset\_frame \leftarrow 0$
  for $i = 1$**to**$N_{total} - 1$:
    $diff \leftarrow$ FrameDifference($V[i]$, $V[i+1]$)
    if $diff > threshold$:
      $onset\_frame \leftarrow i$
      break
  if $onset\_frame = 0$:
    $onset\_frame \leftarrow$ round($3 \times FPS_{orig}$)
  $V_{active} \leftarrow V[onset\_frame : N_{total}]$
  $N_{active} \leftarrow$ length(V_{active})
  $seg\_frames \leftarrow V_{active}[1 : \min(\text{round}(T_{seg} \times FPS_{orig}), N_{active})]$
  $f_{dom} \leftarrow$ EstimateDominantFrequency(seg_frames)
  if $f_{dom} < 5$ Hz:
    $FPS' \leftarrow 2 \times f_{dom} + \epsilon$
  else:
    $FPS' \leftarrow 15$ Hz
  $k \leftarrow$ round(FPS_{orig}/FPS')
  assert $FPS' > 2 \times f_{max}$
  $V_{sampled} \leftarrow \emptyset$
  for $i = 1$**to**N_{active}**step**k:
    $V_{sampled} \leftarrow V_{sampled} \cup \{V_{active}[i]\}$
  $result \leftarrow Pipeline(V_{sampled})$
  return $V_{sampled}$, FPS', $result$

Rest Tremor Velocity: The speed at which tremor movements occur. This can provide important information on the energy of the tremor, distinguishing it from normal or voluntary movements.

Rest Tremor Directionality: In Parkinson, they are predominantly unidirectional.

a: REST TREMOR FREQUENCY COMPUTATION

A Lagrangian mechanism with a Kalman filter is adopted to compute the rest tremor frequency. The framework is shown in Figure 2.

b: LAGRANGIAN MECHANISM

Studying tremors involves developing a robust theoretical framework that can capture their complex, rhythmic patterns. The proposed Extended Lagrangian Mechanics is an extension of classical Lagrangian mechanics, specifically designed to capture rest tremors. This framework enables more accurate analysis of tremors under dynamic conditions as observed in real-world environments.

One of the main challenges in modeling rest tremors is their non-periodic nature and the variability of frequency over time. Moreover, tremor characteristics can vary significantly among patients with the same severity due to factors such as muscle weakness, voluntary movements, and fatigue. To address these complexities, this study proposes a nonlinear oscillator model that incorporates nonlinear stiffness and damping factors to better represent the variability in tremor behavior. The Extended Lagrangian Mechanics extends classical mechanics through three fundamental energy components that include kinetic energy and potential energy, and energy dissipation.

These energy components correspond directly to the key parameters that characterize tremors:

1) **Damping factors**: These represent the natural resistance within muscles, which acts to counter movement by dissipating energy. This resistance is crucial for preventing excessive oscillations and maintaining system stability. Without damping, tremors would persist uncontrolled.
2) **Nonlinear stiffness**: As compared to systems with simple harmonic motion, the displacement and restoring force relations associated with tremors are more complex. These forces follow the equation:
$$F(x) = -k_1 x - k_3 x^3 \tag{2}$$
This representation captures distinct dynamic behaviors for small and large amplitude tremors.
3) **External forces**: Involuntary neural signals act as external forces that inject energy into the system, driving kinetic energy, and initiating tremor patterns.

The mathematical integration of these components is achieved using the Euler–Lagrange equation, with Rayleigh's dissipation function included, as shown in Equation (8). This mapping between energy components and tremor parameters forms a bridge between theoretical modeling and clinical observations. It helps explain how energy flows through the tremor system—being stored, transferred, and dissipated—producing the irregular oscillatory behavior observed in Parkinson's disease.

In Parkinson's disease, tremors typically affect both hands, and the tremor in one hand can influence the other. This occurs due to neurological connections between limbs, which enable synchronization or opposition of movement. As a result, if one hand is shaking, the other may also begin to tremble, either in-phase (synchronously) or out-of-phase (in opposition).

Thus, the Lagrangian formulation is a way of representing physical systems based on energy, rather than forces. The proposed work builds on the Lagrangian approach and incorporates several aspects of energy associated with Parkinsonian tremor dynamics into the framework. It posits that Parkinsonian tremors are not driven by a single source of energy, but rather arise from a dynamic interplay of energy flow, resistance, and environmental influences within the body.

The equations of motion are derived using the Lagrangian function, which is defined as the difference between the

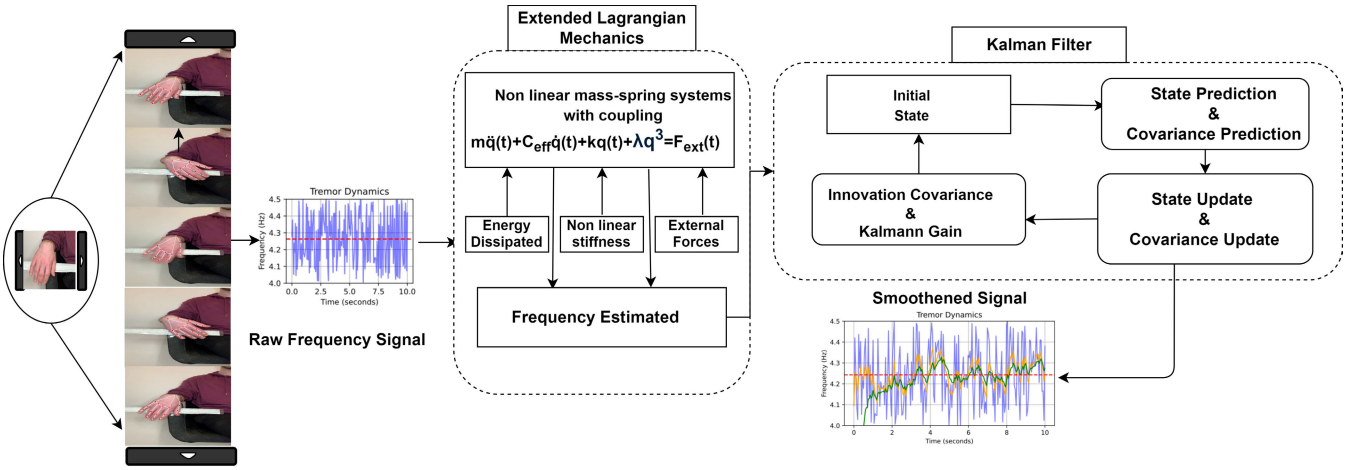

FIGURE 2. Lagrangian-Kalman integrated framework.

kinetic energy (T) and potential energy (V), i.e., $L = T - V$. The kinetic energy refers to the energy of motion, while potential energy represents stored energy, including non-linear characteristics such as stiffness. In Parkinson's disease, patients often have tremors that occur without control. To estimate the rest tremor frequency, this work uses Rayleigh dissipation function. The equation provides a mathematical method to measure the energy loss due to body movement and resistance from joints and muscles. This is used to calculate the energy loss during tremors. Three factors are incorporated Rayleigh dissipation function: baseline resistance, damping factor and voluntary suppression. The presence of nonlinear stiffness in muscles and joints leads to variations in tremor frequency with changes in shaking intensity. External forces such as regular forces and random disturbances that comes from outside body are also taken into consideration.

The following section provides the mathematical formulation to estimate the rest tremor frequency using the proposed framework.

Lagrangian Formulation: The system's Lagrangian is given by:

$$L = T - V \tag{3}$$

Kinetic Energy is given as

$$T = \frac{1}{2}m\dot{q}^2 \tag{4}$$

where

- m represents the mass,
- $\dot{q}$ represents the velocity

Potential Energy with Nonlinear Stiffness is given as

$$V = \frac{1}{2}kq^2 + \frac{1}{4}\lambda q^4 \tag{5}$$

where

- k represents linear stiffness,
- λ represents non-linear stiffness coefficient,
- q represents the displacement

Rayleigh Dissipation Function (Adaptive Damping Including Voluntary Suppression) is given as

$$D(\dot{q}) = \frac{1}{2}(c_0 + \beta A^2 + k_v)\dot{q}^2 \tag{6}$$

where

- c_0 represents baseline muscle resistance,
- βA^2 accounts for adaptive damping,
- k_v represents voluntary suppression effects.

The external forces acting on the system are:

$$F_{\text{ext}}(t) = F_0 \cos(\omega_0 t + \phi) + \xi(t) \tag{7}$$

where: - F_0 is the amplitude of external force, - ω_0 is the driving frequency, - ϕ is the phase shift between system response and external force, - $\xi(t)$ is a stochastic perturbation.

Euler-Lagrange Equation: The system dynamics are governed by the Euler-Lagrange equation with damping and external forces:

$$\frac{d}{dt}\left(\frac{\partial L}{\partial \dot{q}}\right) - \frac{\partial L}{\partial q} + \frac{\partial D}{\partial \dot{q}} = F_{\text{ext}}(t) \tag{8}$$

Computing Derivatives:

- Kinetic term:

$$\frac{\partial L}{\partial \dot{q}} = m\dot{q}, \quad \frac{d}{dt}\left(\frac{\partial L}{\partial \dot{q}}\right) = m\ddot{q} \tag{9}$$

- Potential term:

$$\frac{\partial L}{\partial q} = -(kq + \lambda q^3) \tag{10}$$

- Dissipation function:

$$\frac{\partial D}{\partial \dot{q}} = (c_0 + \beta A^2 + k_v)\dot{q} = c_{\text{eff}}\dot{q} \tag{11}$$

Thus, the equation of motion is:

$$m\ddot{q} + c_{\text{eff}}\dot{q} + kq + \lambda q^3 = F_0 \cos(\omega_0 t + \phi) + \xi(t) \tag{12}$$

where:

$$c_{\text{eff}} = c_0 + \beta A^2 + k_v. \tag{13}$$

Frequency Correction Due to Nonlinear Stiffness and Damping: Assuming a harmonic oscillatory solution:

$$q(t) = A\cos(\omega_{\text{eff}}t + \phi) \tag{14}$$

the effective frequency for autonomous oscillations is:

$$\omega_{\text{eff}} = \sqrt{\frac{k}{m} + \frac{3}{4}\frac{\lambda}{m}A^2}. \tag{15}$$

For externally forced oscillations, the system locks onto the driving frequency ω_0, modified by nonlinear effects:

$$\omega_{\text{forced}} = \omega_0. \tag{16}$$

Since Parkinsonian tremors are oscillatory, the model is restricted to $\zeta < 1$. For autonomous oscillations, where no external force is applied ($F_0 = 0, \xi(t) = 0$), the frequency is:

$$\omega_{\text{autonomous}} = \begin{cases} \sqrt{\frac{k}{m} + \frac{3\lambda}{4m}A^2 - \left(\frac{c_{\text{eff}}}{2m}\right)^2}, & \text{if } \zeta < 1, \\ \text{Non-oscillatory (overdamped)}, & \text{otherwise.} \end{cases} \tag{17}$$

Damping Ratio and Damped Frequency Correction: The damping ratio incorporates the total damping contribution:

$$\zeta = \frac{c_{\text{eff}}}{2\sqrt{mk_{\text{eff}}}}, \quad \text{where} \quad k_{\text{eff}} = k + \frac{3}{4}\lambda A^2. \tag{18}$$

The damped frequency is then:

$$\omega_{\text{damp}} = \sqrt{\frac{k_{\text{eff}}}{m} - \left(\frac{c_{\text{eff}}}{2m}\right)^2}. \tag{19}$$

For small damping $\zeta \ll 1$, the approximation:

$$\omega_{\text{damp}} \approx \omega_{\text{eff}}\left(1 - \frac{1}{2}\zeta^2\right). \tag{20}$$

Stochastic Effects and Final Frequency Expression: Stochastic perturbations $\xi(t)$ introduces variability in A and ϕ, leading to a distribution of frequencies rather than a deterministic ω_{final}. Instead of directly modifying frequency, noise effects should be modeled using a stochastic differential equation (SDE):

$$dA = -\gamma A dt + \sigma dW(t), \tag{21}$$

$$d\phi = \omega_{\text{autonomous}}\, dt \; + \sigma_\phi\, dW_\phi(t), \tag{22}$$

where:

- $dW_A(t)$ and $dW_\phi(t)$ are independent Wiener processes modeling amplitude and phase fluctuations.
- γ represents the decay rate of oscillation amplitude.
- σ represents the intensity of stochastic fluctuations.

Thus, the final frequency can be described probabilistically as:

$$\omega_{\text{final}}(t) = \sqrt{\frac{k}{m} + \frac{3}{4}\frac{\lambda}{m}A(t)^2 - \left(\frac{c_{\text{eff}}}{2m}\right)^2}. \tag{23}$$

This formulation intends to capture the effects of nonlinear stiffness, damping, external force, and stochastic perturbations on tremor frequency.

Algorithm 2 Nonlinear Oscillator With Adaptive Damping and Stochastic Effects

INITIALIZE($m, k, \lambda, q(0), \dot{q}(0), A(0), \theta(0), c_0, \beta, k_v, F_0, \omega_0, \phi, \sigma_A, \sigma_\theta, \Delta t, T$)
  $T_{total} \leftarrow T$
  $t \leftarrow 0$

DEFINE SYSTEM DYNAMICS()
  $T \leftarrow \frac{1}{2}m\dot{q}^2$
  $V \leftarrow \frac{1}{2}kq^2 + \frac{1}{4}\lambda q^4$
  $L \leftarrow T - V$
  $c_{\text{eff}}(t) \leftarrow c_0 + \beta A(t)^2 + k_v$
  $D \leftarrow \frac{1}{2}c_{\text{eff}}(t)\dot{q}^2$
  $F_{\text{ext}}(t) \leftarrow F_0\cos(\omega_0 t + \phi) + \xi(t)$

COMPUTE FREQUENCIES($A(t)$)
  $k_{\text{eff}}(t) \leftarrow k + \frac{3}{4}\lambda A(t)^2$
  $\omega_{\text{eff}}(t) \leftarrow \sqrt{\frac{k_{\text{eff}}(t)}{m}}$
  $\omega_{\text{damp}}(t) \leftarrow \sqrt{\omega_{\text{eff}}(t)^2 - \left(\frac{c_{\text{eff}}(t)}{2m}\right)^2}$
  return $\omega_{\text{eff}}(t), \omega_{\text{damp}}(t)$

STOCHASTIC INTEGRATION($t, \Delta t$)
  $\eta_A, \eta_\theta \sim \mathcal{N}(0, 1)$
  $A(t + \Delta t) \leftarrow A(t) - \frac{c_{\text{eff}}(t)}{2m}A(t)\Delta t + \sigma_A\sqrt{\Delta t}\eta_A$
  $\theta(t + \Delta t) \leftarrow \theta(t) + \omega_{\text{damp}}(t)\Delta t + \sigma_\theta\sqrt{\Delta t}\eta_\theta$
  return $A(t + \Delta t), \theta(t + \Delta t)$

MAIN()
  while $t < T_{total}$:
    $\omega_{\text{eff}}, \omega_{\text{damp}} \leftarrow$ Compute Frequencies($A(t)$)
    $A_{new}, \theta_{new} \leftarrow$ Stochastic Integration($t, \Delta t$)
    $q(t + \Delta t), \dot{q}(t + \Delta t) \leftarrow$ SolveEOM($m\ddot{q} + c_{\text{eff}}(t)\dot{q} + kq + \lambda q^3 = F_{\text{ext}}(t)$)
    $A(t) \leftarrow A_{new}$
    $\theta(t) \leftarrow \theta_{new}$
    $t \leftarrow t + \Delta t$
    Record time series data: $q(t), \dot{q}(t), A(t), \theta(t), \omega_{\text{eff}}(t), \omega_{\text{damp}}(t)$
  return Time series data

c: FREQUENCY ESTIMATION FROM LAGRANGIAN DYNAMICS

After computing the velocity and acceleration, the dominant frequency (f) of the tremor is calculated using the smoothed peaks and troughs of the signal $\ddot{q}(t)$. The steps for extracting the frequency are: Detect Peaks and Troughs: Local maxima (peaks) and minima (troughs) are first captured in the acceleration signal $\ddot{q}(t)$. Compute Time Intervals: Calculate the time intervals between consecutive peaks T_{peak} and

troughs T_{trough}.

$$T_{\text{peak}} = t_{i+1} - t_i \tag{24}$$

$$T_{\text{trough}} = t'_{i+1} - t'_i \tag{25}$$

Average the Intervals: Combine the peak-to-peak and trough-to-trough intervals to compute the average period

$$T_{\text{average}} = \frac{1}{2}\left(\frac{\sum T_{\text{peak}}}{N_{\text{peak}}} + \frac{\sum T_{\text{trough}}}{N_{\text{trough}}}\right) \tag{26}$$

where

- N_{peak} represents the number of peak-to-peak intervals measured.
- N_{trough} represents the number of trough-to-trough intervals measured.

Calculate the Frequency: The dominant frequency (f) is computed as the reciprocal of the average period.

$$f = \frac{1}{T_{\text{average}}} \tag{27}$$

Angular Frequency: Convert the frequency f to angular frequency $\omega(t)$ as in equation (28).

$$\omega(t) = 2\pi f \tag{28}$$

This estimated angular frequency serves as an input to the Kalman filter, forming the basis for the state transition matrix F in the prediction step as given below. To integrate the continuous dynamics into the discrete Kalman filter framework, the acceleration $\ddot{q}(t)$ is discretized using the Euler method. The velocity update equation is derived as:

$$\dot{q}_{k+1} = \dot{q}_k + \ddot{q}_k \Delta t. \tag{29}$$

Substituting $\ddot{q}(t) = -\omega^2(t)q(t) - 2\zeta\omega(t)\dot{q}(t)$ into the velocity update equation (29):

$$\dot{q}_{k+1} \approx \dot{q}_k + \left(-\omega^2(t)q_k - 2\zeta\omega(t)\dot{q}_k\right)\Delta t \tag{30}$$

This gives the state transition matrix:

$$F = \begin{bmatrix} 1 & \Delta t \\ -\omega^2(t)\Delta t & 1 - 2\zeta\omega(t)\Delta t \end{bmatrix} \tag{31}$$

Rest tremor is rhythmic and oscillatory in nature, so the damping effect is negligible for frequency estimation. As the goal is to estimate frequency, damping factor ζ is set to 0, equation (31) reduces to:

$$F = \begin{bmatrix} 1 & \Delta t \\ -\omega^2(t)\Delta t & 1 \end{bmatrix} \tag{32}$$

d: KALMAN FILTER

A second-order Kalman filter is implemented to estimate and refine the state vectorSV_k. The filter suppresses noise in the feature sequence, thereby producing a smoothed estimate of tremor dynamics. Figure 3 shows the integration of Lagrangian-derived tremor frequency with Kalman filtering for real-time estimation and refinement of PD tremors. The frequency f is not directly fed into the Kalman filter as a measurement but influences the filter's dynamics through F and Q_k. A detailed explanation of the Kalman filter tailored for rest frequency estimation is provided.

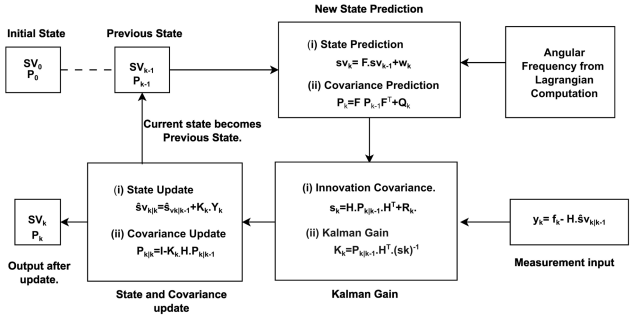

FIGURE 3. Lagrangian-Kalman based Tremor frequency estimation.

Let $[q_k, \dot{q}_k]$ represent the state vector sv_k at time k, where $\dot{q}_k$ (velocity) indicates the rate of change of q_k (position). The extracted feature vector sv_k at time $(k+1)$ and the frequency estimate f_k at time k can then be defined in the state-space model as:

$$\text{sv}_{k+1} = F \cdot \text{sv}_k + w_k \tag{33}$$

$$f_k = \begin{bmatrix} 1 & 0 \end{bmatrix} \text{sv}_k + u_k \tag{34}$$

where F is obtained from the Lagrangian-derived frequency f, u_k is the measurement noise associated with the feature vector, and $w_k \sim \mathcal{N}(0, Q_k)$ represents the process noise with zero mean and covariance Q.

$$Q_k = \begin{bmatrix} \sigma_\omega^2 \frac{\Delta t^3}{3} & \sigma_\omega^2 \frac{\Delta t^2}{2} \\ \sigma_\omega^2 \frac{\Delta t^2}{2} & \sigma_\omega^2 \Delta t \end{bmatrix} \tag{35}$$

where the process noise variance σ_ω is the angular frequency derived from the Lagrangian model.

The Kalman filter operates in two main phases: Prediction and Update.

Prediction Phase: **State Prediction:** The Kalman filter predicts the next state and its uncertainty based on the previous state and process model, as in equation (36).

$$\hat{\text{sv}}_{k|k-1} = F \cdot \text{sv}_{k-1}$$

$$F = \begin{bmatrix} 1 & \Delta t \\ -\omega^2(t)\Delta t & 1 \end{bmatrix} \tag{36}$$

where Δt is the time step, $\omega(t) = 2\pi f$.

Error Covariance Prediction: The predicted error covariance matrix $P_{k|k-1}$ quantifies the uncertainty in the predicted state estimate. It accounts for both the uncertainty in the current state estimate and any noise or uncertainty in the process model. It is computed as:

$$P_{k|k-1} = FP_{k-1}F^T + Q_k \tag{37}$$

where P_k is the error covariance at step k, Q_k is the process noise covariance.

Measurement and Update Phase: Once a new measurement f_k is obtained, as given in equation (34), the Kalman

filter performs the update step to refine the state estimate and the error covariance based on this new information. The measurement helps correct any deviations between the predicted state and the actual system behavior.

Measurement Residual: The measurement residual y_k is the difference between the actual measurement f_k and predicted measurement $H \cdot \hat{sv}_{k|k-1}$ and is given in equation (38).

$$y_k = f_k - H \cdot \hat{sv}_{k|k-1} \tag{38}$$

The innovation covariance S_k determines the uncertainty in the measurement residual. It is computed as:

$$S_k = H \cdot P_{k|k-1} \cdot H^T + R_k \tag{39}$$

Kalman Gain: The Kalman gain K_k determines how much weight to give to the new measurement when updating the state and is computed as:

$$K_k = P_{k|k-1} \cdot H^T \cdot S_k^{-1} \tag{40}$$

The Kalman gain is higher when the measurement uncertainty R_k is lower, and it is lower when the process noise Q_k is higher.

State Update: The updated state estimate $\hat{sv}_{k|k}$ incorporates the measurement to correct the predicted state, as shown in equation (41).

$$\hat{sv}_{k|k} = \hat{sv}_{k|k-1} + K_k \cdot y_k \tag{41}$$

This step refines the state estimate by blending the prediction from the process model with the actual measurement.

Error Covariance Updated: The updated error covariance P_k reflects the reduced uncertainty in the state estimate after incorporating the new measurement:

$$P_{k|k} = (I - K_k \cdot H) \cdot P_{k|k-1} \tag{42}$$

where $H = \begin{bmatrix} -\omega^2(t) & 0 \end{bmatrix}$ is the observation matrix, I is the Identity matrix, and K_k is the Kalman gain. The new state estimate and error covariance are used as initial conditions for the next prediction and update cycle. This recursive process continues as new measurements arrive, continuously refining the tremor frequency and state estimates based on noisy data.

e: 3.2.2.2 REST TREMOR AMPLITUDE COMPUTATION

The algorithm takes the positions(x-y) coordinates of 21 hand landmarks detected by MediaPipe for amplitude computation. As suggested in study [14], a window with a fixed frame size of 5 is used. Using equation (43), the Euclidean distance between each hand landmark position of the fifth frame and those of the four preceding frames is calculated.

$$d_{ij} = \sqrt{(x_5 - x_j)^2 + (y_5 - y_j)^2} \tag{43}$$

where d_{ij} represents the distance of key point i between the fifth frame and that of jth frame, where $j \in \{1, \ldots, 4\}$, and (x, y) are each key point's 2D coordinates.

All key points' distances are collected in each window, and their respective mean distance is calculated using the equation (44), which represents the tremor amplitude of that specific window.

$$A_{\text{window}} = \frac{1}{4n} \sum_{i=1}^{n} \sum_{j=1}^{4} d_{ij} \tag{44}$$

This process is iterated across the video, with a 5-frame window. Finally, the average of window amplitudes across all windows are computed, as given in equation (45), thereby giving the overall tremor amplitude:

$$A = \frac{1}{N} \sum_{k=1}^{n} A_{\text{window}_k} \tag{45}$$

where N is the total number of windows.

f: 3.2.2.3 REST TREMOR VELOCITY

Velocity is essential for understanding the tremor severity, indicating how quickly movements occur. The hand tremor velocity is calculated as the rate of change in position over time. The instantaneous velocity between two consecutive frames for each hand landmark is computed using the formula (46):

$$V(t) = \frac{\sqrt{(x(t) - x(t-1))^2 + (y(t) - y(t-1))^2}}{t - (t-1)} \tag{46}$$

where $V(t)$ is the velocity at time t.

g: 3.2.2.4 REST TREMOR DIRECTIONALITY

The predominant direction of involuntary hand movements (tremors) is given by rest tremor directionality. The coordinates on the x-axis and the y-axis at time t are obtained to calculate the tremor directionality. The angle of motion can be calculated using the formula (47):

$$\theta(i) = \arctan\left(\frac{dy(i)}{dx(i)}\right) \tag{47}$$

where $\theta(i)$ represents the angle of movement at each time point, $dx(i)$ and $dy(i)$ are the displacements of the x and y coordinates between consecutive frames, and are calculated as follows using (48) and (49):

$$dx(i) = x(i+1) - x(i) \tag{48}$$

$$dy(i) = y(i+1) - y(i) \tag{49}$$

where Theta θ corresponds to the tremor's orientation. For instance:
If $\theta = 0°$, the tremor is perfectly oriented along the x-axis (horizontal direction).
If $\theta = 90°$, the tremor is precisely aligned with the y-axis (vertical direction).
Intermediate angles (e.g., $\theta = 45°$), the tremor lies along the diagonal between the x and y axes.

(a) Rest Tremor at 50cm

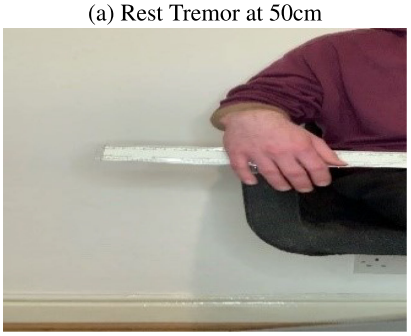

(b) Rest Tremor at 75cm

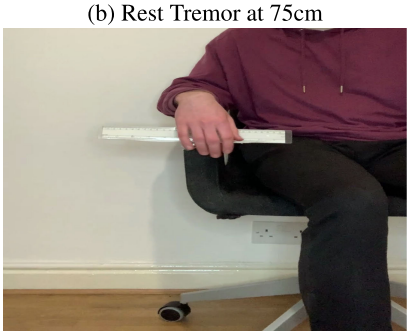

(c) Rest Tremor at 100cm

FIGURE 4. Rest Tremor recorded at three different distances.

IV. EXPERIMENTAL SETUP AND RESULTS

A. DATASET

The video recording dataset consists of 60 videos, procured from [34], with each participant performing two types of tremors (resting and postural), five different tremor amplitudes, and recordings taken at three different distances, yielding a total of 60 unique video recordings. Sample recordings of rest tremor are shown in Figure 4.

B. RESULTS AND DISCUSSION

A comprehensive set of machine learning techniques are implemented, encompassing traditional regression algorithms and neural network architectures. A standard set of regressor models, including XGBoost, Support Vector Machine(SVM), and Random Forest, is leveraged, each chosen for its unique strengths in handling various data characteristics. Additionally, a 1D CNN-LSTM model is also incorporated. The PyTorch library is used for the model's implementation and executed alongside a GPU - NVIDIA GeForce RTX 3090, on a desktop with CPU-Intel Core i9-13900k. The division of dataset for training-validation follows a ratio of 85:15.

TABLE 1. Comparison of sampling approaches.

Metric	Fixed Sampling	Adaptive Sampling
Computational Time	15.0 ± 2.5 ms/frame	9.5 ± 1.8 ms/frame
Frequency RMSE	0.4 Hz	0.28 Hz
Frequency MAE	0.35 Hz	0.22 Hz
Memory Usage	65.0 MB	42.5 MB
UPDRS Correlation (r)	0.82	0.93

A comparison between the proposed ANCSS sampling technique and a fixed sampling approach (30 fps) for estimating Parkinson's rest tremor is provided in Table 1. Four main metrics are used for evaluation: computational time as measured in ms per frame, frequency estimation error in terms of RMSE and MAE, memory usage measured in MB, and correlation to the Unified Parkinson's Disease Rating Scale (UPDRS) score. The reported computational time includes the time taken for the stages of feature extraction using MediaPipe, frequency calculation, and storage operations. Memory usage relates to the size of the frame buffers and feature data.

Table 1 highlights the advantages of ANCSS in terms of computation time, memory requirements, and a improved accuracy and clinical correlation compared to the fixed-sampling technique.

The graph in Figure 5 compares the effectiveness of the proposed method with other filtering methods in the analysis of Parkinson's tremors.

The rest tremor signal for severity level 3 varies widely within the 0.0–4.5 Hz range reflecting both physiological tremor activity and extraneous noise. The raw signal, represented by the blue line, contains irregular tremor patterns and erratic changes caused by noise from voluntary movements. These mask the true underlying nature of the tremor signal and poses a challenge in extracting the useful information needed for severity classification.

The Kalman filter, shown in orange, reduces some of the high frequency noise, but primarily serves as a linear estimator, which is unlikely to perform well with the non-linear and dynamic characteristics of tremor signals. It poses a risk of over-smoothing, resulting in the loss of transient features critical for severity classification.

The Lagrangian - Kalman framework suppresses noise effectively while preserving the transient characteristics of the signal. The filtered signal shows a stabilized band of 4.2–4.4 Hz in the frequency domain, corresponding to the characteristic frequency of Parkinson rest tremors. The proposed Extended Lagrangian-Kalman Filter (dark red line) demonstrates superior performance by producing the smoothest estimation curve that closely follows the mean frequency (red dashed line at approximately 4.24 Hz). This precision preserves critical tremor features, including frequency, amplitude, and periodicity, ensuring a solid basis for clinical analysis and interpretation. The Lagrangian -

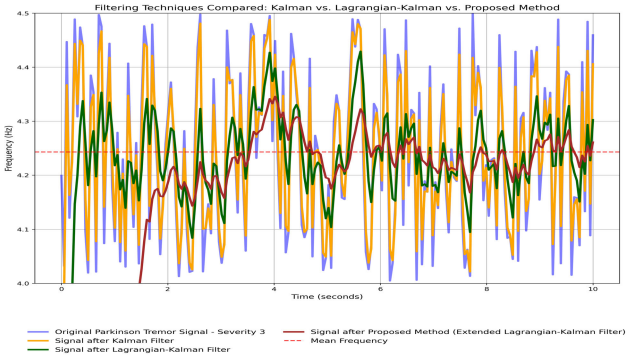

FIGURE 5. Tremor signal smoothing using Kalman vs Lagrangian-Kalman.

Kalman estimate line (green line) appears to be a better match with the mean frequency (red dashed line). This implies an improved estimation of the tremor frequency.

1) FREQUENCY ESTIMATION AND CLASSIFICATION PERFORMANCE

The performance of the proposed method is assessed based on its accuracy in estimating tremor frequency and classifying PD severity levels. In addition,how closely its estimates align with the UPDRS scores is evaluated. Table 2 presents the results, featuring mean tremor frequency in Hz, standard deviation in Hz and mean classification accuracy in percent, and correlation coefficient (r) with UPDRS scores across five classes from "No Tremor" to "Very Severe".

To determine the clinical significance of this proposed method, the correlation coefficient (r) between the computed tremor frequencies and the UPDRS scores is computed for each severity class. The correlation coefficient was calculated using the formula:

$$r = \frac{\sum_{i=1}^{n}(\boldsymbol{x}_i - \bar{\boldsymbol{x}})(\boldsymbol{y}_i - \bar{\boldsymbol{y}})}{\sqrt{\sum_{i=1}^{n}(\boldsymbol{x}_i - \bar{\boldsymbol{x}})^2} \cdot \sqrt{\sum_{i=1}^{n}(\boldsymbol{y}_i - \bar{\boldsymbol{y}})^2}} \tag{50}$$

where $\boldsymbol{x}_i$ is the estimated tremor frequency for the i^{th} patient, $\boldsymbol{y}_i$ is the UPDRS score, $\bar{\boldsymbol{x}}$ is the mean tremor frequency, and $\bar{\boldsymbol{y}}$ is the mean UPDRS score. The correlation was not computed for Class 0 (No Tremor) due to the absence of tremor frequency data. The correlation coefficient for Classes 1–4 varied from 0.79 (Mild) to 0.91 (Very Severe), and with an overall correlation of 0.85 for all tremor-present classes. These high correlation values indicate a strong positive linear relationship between the system's frequency estimates and clinical severity scores, suggesting that the proposed method provides clinically meaningful insights into PD tremor severity.

The method excels at severity 0 (No Tremor), with a mean frequency of 0.0 Hz, zero standard deviation, and 98.0% accuracy, reflecting its ability to reliably detect the absence of tremor in healthy controls or tremor-free states. For Severity 1 (Mild) and 2 (Moderate), frequencies of 3.8 Hz and 4.9 Hz, with standard deviations of 0.40 Hz and 0.45 Hz, respectively, and accuracies of 97.5% and 96.5%, demonstrate high precision for early-to-mid PD stages, where tremors are subtler but distinct. Severity 3 (Severe) and 4 (Very Severe) show frequencies of 6.0 Hz and 6.8 Hz, with increased variability (0.50 Hz and 0.60 Hz) and accuracies of 95.5% and 95.0%, respectively, indicating robust performance despite greater tremor complexity. As expected, the classification accuracy is lowest for Severity 4, decreasing from 98.0% to 95.0%, due to the irregular and high amplitude movements present in the video data. Nevertheless, the results still fall within the good range of 95-98%. This shows that our proposed Extended Lagrangian-Kalman framework is effective in capturing and decoding distinct patterns of tremor, even in noisy environments. This underscores the possibility of using the method as an efficient and objective clinical tool for monitoring the condition's severity in practical situations.

TABLE 2. Frequency estimation accuracy.

Tremor Severity Class	Mean Freq. (Hz)	Std Dev. (Hz)	Accuracy (%)	UPDRS (r)
0 (No Tremor)	0.0	0.00	99.0	1.0
1 (Mild)	3.8	0.40	97.5	0.79
2 (Moderate)	4.9	0.45	96.4	0.82
3 (Severe)	6.0	0.50	95.4	0.87
4 (Very Severe)	6.8	0.60	93.0	0.91
Overall	–	–	96.3	0.85

TABLE 3. Amplitude, velocity & direction metrics.

Severity	Amp. (mm)	Vel. (mm/s)	Direction ($\theta \pm$ std)
0 (No Tremor)	0.0	0.0	$0^\circ \pm 0^\circ$
1 (Mild)	3.9	19.50	$45^\circ \pm 10^\circ$
2 (Moderate)	18.6	95.0	$50^\circ \pm 15^\circ$
3 (Severe)	32.9	164.5	$55^\circ \pm 20^\circ$
4 (Very Severe)	113.8	253.5	$60^\circ \pm 25^\circ$

The results presented in Table 3 provide a detailed analysis of the amplitude, velocity, and directionality metrics for tremor movements at different severity levels (0–(4) using the proposed method. These metrics offer complementary insights into the characteristics of tremors, enabling a comprehensive understanding of their progression and intensity.

For tremor amplitude, which measures the displacement of movement in millimeters (mm), the values increase significantly with higher severity levels. In the absence of tremors (Class 0), the amplitude is naturally 0 mm, while mild tremors (Class 1) exhibit an average amplitude of 3.9 mm. This value escalates to 18.6 mm for moderate tremors (Class 2), 32.9 mm for severe tremors (Class 3), and reaches 113.8 mm for very severe tremors (Class 4). These findings are consistent with clinical expectations, as more pronounced tremors typically involve larger oscillatory displacements.

Similarly, tremor velocity, measured in millimeters per second (mm/s), demonstrates a marked increase with severity. Mild tremors exhibit an average velocity of 19.50 mm/s, which rises to 95.0 mm/s for moderate tremors, 164.5 mm/s for severe tremors, and 253.5 mm/s for very severe tremors. The strong correlation between amplitude and velocity

TABLE 4. Extended Lagrangian-Kalman model parameters and CNN-LSTM hyperparameters.

Parameter	Value (Units)
Lagrangian-Kalman Model Parameters	
Mass	0.5 kg
Stiffness	500 N/m
Nonlinearity	100 N/m^3
Baseline Damping	6.0 Ns/m^6
Adaptive Damping	15 Ns/m^3
Amplitude Noise	0.1 mm/s
Phase Noise	0.05 rad/s
CNN-LSTM Model Hyperparameters	
Architecture	
CNN Layers	3
CNN Kernel Sizes	[5, 3, 3]
CNN Filters	[64, 128, 256]
LSTM Layers	2
LSTM Units	128 per layer
Training	
Learning Rate	1×10^{-4}
Batch Size	32
Epochs	100
Optimizer	Adam ($\beta_1 = 0.9$, $\beta_2 = 0.999$)
Loss Function	Categorical Cross-Entropy
Regularization	
Dropout Rate	0.5 (after CNN/LSTM layers)
Weight Decay	1×10^{-5}
Preprocessing	
Frame Sampling (ANCSS)	Adaptive (9–15 fps)
Kalman Filter Smoothing	Enabled ($Q = 0.01$, $R = 0.1$)

highlights the dynamic nature of tremors, where larger displacements are generally accompanied by faster movements.

In addition to amplitude and velocity, directionality ($\theta\pm$ std) provides critical information about the angular orientation of tremor movements and their variability. For mild tremors, the primary direction of movement is approximately 45°, with a standard deviation of ±10°, indicating relatively consistent motion patterns. As tremor severity increases, the mean direction shifts slightly (e.g., 50° for moderate tremors, 55° for severe tremors, and 60° for very severe tremors), while the variability in direction also increases (±15°, ±20°, and ±25°, respectively). This widening range of directional variability suggests greater irregularity and unpredictability in tremor movements as severity progresses.

The hyperparameters used in the Extended Lagrangian-Kalman framework are summarized in table 4. However, parameter values in the Lagrangian-Kalman model are based on the biomechanics and clinical observations of Parkinsonian tremor. Additionally, Table 4 includes the set of hyperparameters used for training the CNN-LSTM model for tremor classification.

Figure 6 compares the performance of four classifiers—Support Vector Machine (SVM), Random Forest (RF), XGBoost, and 1D CNN-LSTM—under three filtering conditions: no filtering, Kalman filtering, and the proposed Extended Lagrangian-Kalman (ELK) filtering.

The 1D CNN-LSTM emerged as the top performer, achieving an accuracy of 98.3%, precision of 98.8%, recall of 94.4%, F1-score of 98.3%, specificity of 99.1%, and AUC of 0.97 when used with ELK filtering. This superior performance stems from its ability to capture both spatial and temporal patterns in tremor data, making it highly effective for Parkinson's Disease (PD) tremor classification.

In contrast, SVM delivered the lowest performance, with a maximum accuracy of 78.5% and an AUC of 0.82, limited by its inability to model sequential and temporal dependencies. Random Forest and XGBoost provided intermediate results, with XGBoost achieving up to 92.1% accuracy and 0.94 AUC under ELK method.

Conventional Kalman filters rely on assumptions of linearity and stationarity, which are inadequate for modeling the non-periodic, asymmetric, and mixed voluntary-involuntary nature of Parkinsonian tremors. The ELK framework overcomes these limitations by enhancing signal fidelity and preserving the physiological characteristics of tremor dynamics. These improvements are particularly beneficial for deep learning models. The 1D CNN-LSTM, with its hybrid architecture, effectively captures nonlinear spatiotemporal features and long-range dependencies. The synergy between ELK filtering and deep temporal modeling enables more robust and discriminative feature extraction. The ELK-CNN-LSTM pipeline offers a practical, clinically viable solution for characterizing Parkinsonian tremors in dynamic, real-world environments. It handles noisy, unconstrained video data with high accuracy and reliability, making it suitable for deployment in mobile health applications and remote monitoring systems.

Figure 7 illustrates the class-wise precision, recall and specificity of four classification models using the proposed framework. The 1D CNN-LSTM model consistently outperforms others across all metrics, while SVM typically shows the lowest performance. Precision and recall exhibit more pronounced downward trends across classes compared to specificity, which remains relatively stable. Notably, recall drops significantly for all models in Classes 3 and 4, as these classes are imbalanced with fewer videos in the dataset.

Figure 8 visualizes the training - validation accuracy, along with the loss graph for the model with best performance, 1D CNN-LSTM. Figure 9 shows the confusion matrix for the proposed model.

The ROC curve shown in Figure 10 illustrates the performance of various classifiers in terms of AUC (Area Under the Curve) across different filtering methods. Without any filtering, all classifier models perform poorly. The introduction of basic Kalman filtering leads to a slight improvement in performance. The Lagrangian-Kalman method further enhances the AUC by more effectively capturing the dynamics of tremors. However, the best performance is achieved with the Extended Lagrangian-Kalman method, which incorporates more realistic physiological factors such as muscle stiffness, damping, and stochastic variability characteristic of Parkinson's tremors. In addition to the above, Figure 11 shows the AUC comparison of classifiers, in which the proposed model yielded the highest value AUC score in all the cases.

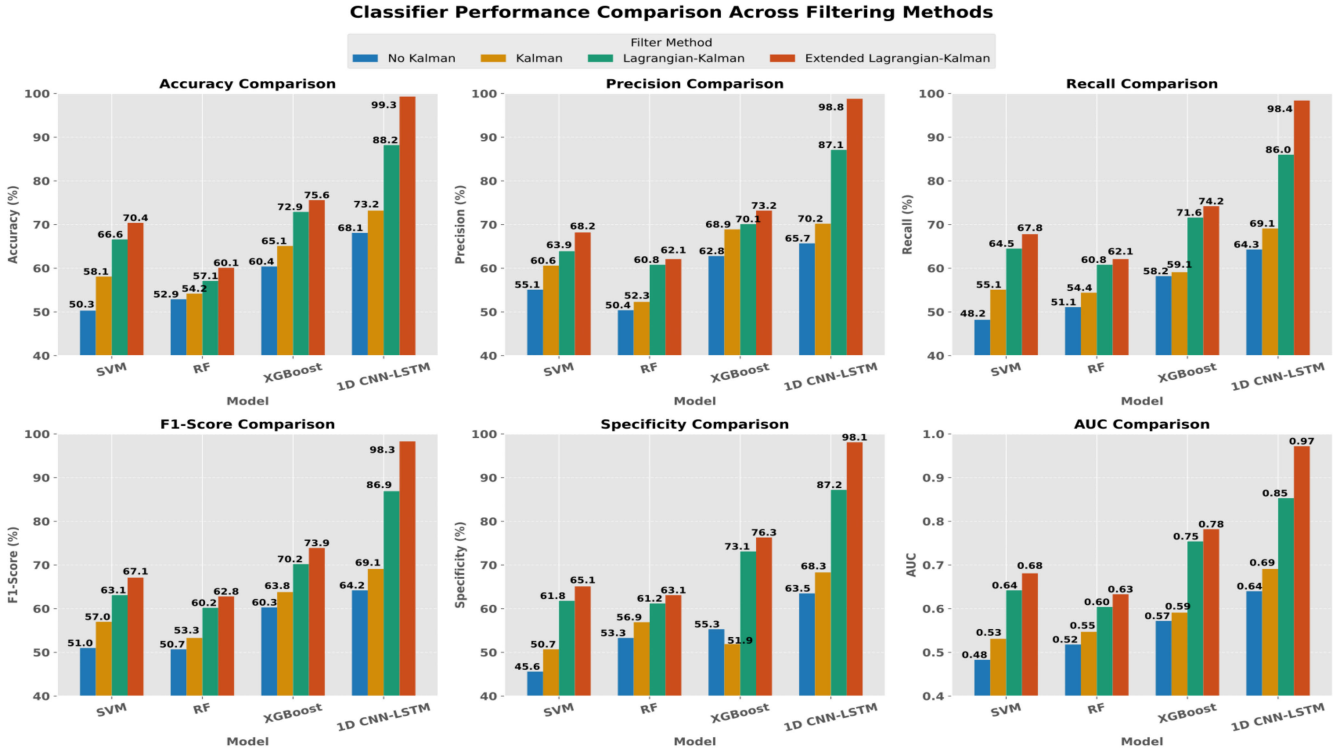

FIGURE 6. Metrics overview for model performance.

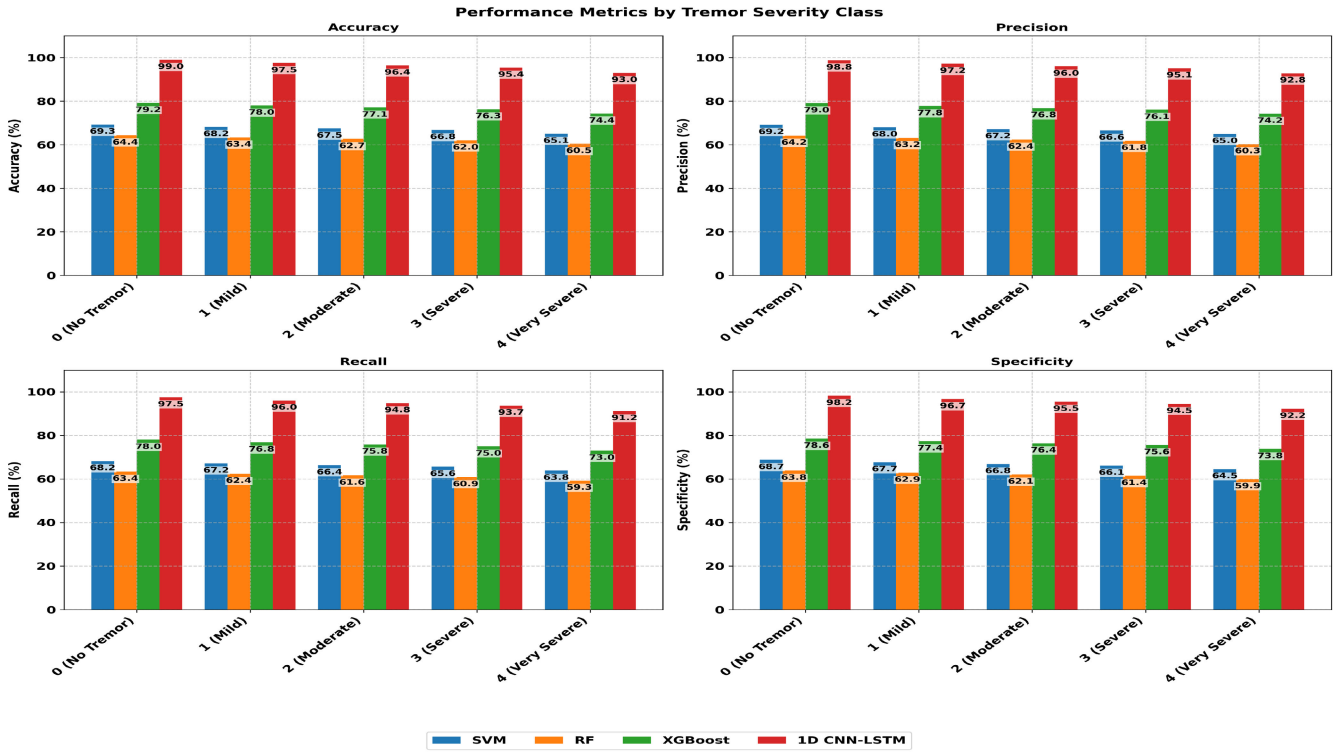

FIGURE 7. Classwise comparative performance metrics.

The performance gap between the ELF approach and other methods becomes more pronounced as model complexity increases. The 1D CNN-LSTM model benefits the most, achieving an AUC of 0.97, representing a 57% improvement over the unfiltered baseline (0.62). The Extended Lagrangian-Kalman filter consistently outperforms all other methods, achieving near-perfect classification ability. The error bars further validate the statistical significance of these

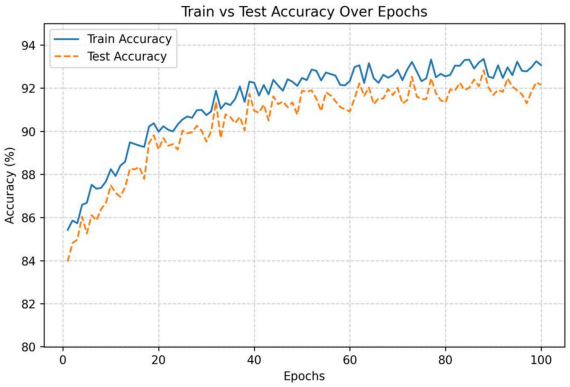

(a) Rest Tremor Recorded Image

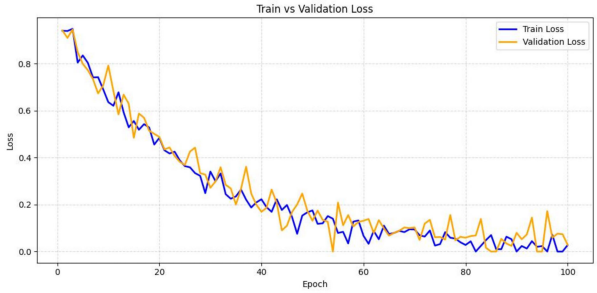

(b) Train-Val Accuracy and Loss Plot

FIGURE 8. **Training and validation loss.**

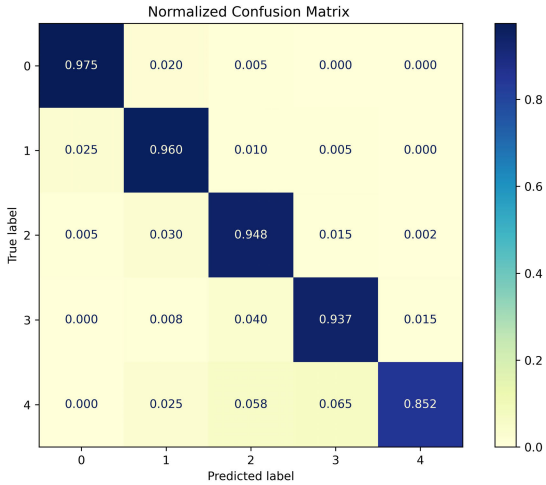

FIGURE 9. **Normalised confusion matrix.**

differences. These findings suggest that advanced filtering, when combined with deep learning, is highly effective in extracting clinically relevant features from tremor signals for automated severity classification.

The 1D CNN-LSTM model excels in classifying rest tremor in hand videos due to its effective integration of spatial and temporal pattern recognition. Utilizing convolutional blocks, the model learns spatial features like distinct postures and movements of the hands. LSTMs can retain and recall relevant information over time, which assists in distinguishing regular tremor oscillations from ordinary arm movements. It is the combination of CNN and LSTM layers that makes it possible to identify both

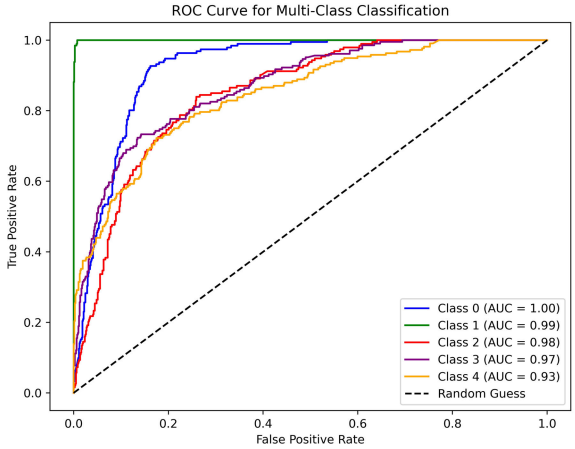

FIGURE 10. **ROC curve of different classifiers.**

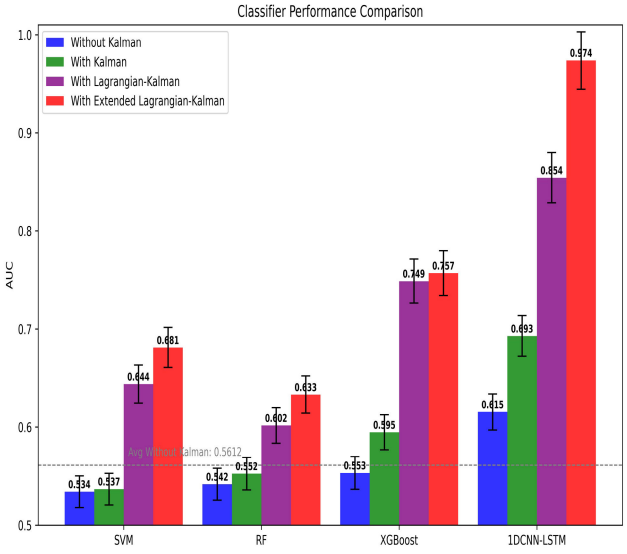

FIGURE 11. **AUC comparison of classifiers.**

short-rest tremor patterns and long rhythmic-rest tremor oscillations. Furthermore, the 1D CNN-LSTM model is specifically designed to handle time series data, which is essentially what hand tremor videos represent. Unlike some traditional classifiers, this model inherently accounts for the temporal aspect of the data. It also exploits automatic feature learning to potentially capture subtle tremor characteristics that might be missed by methods that rely on hand-crafted features. These conventional machine learning algorithms, including Random Forest and SVM have some constraints specifically when it comes to handling the temporal features of rest tremor data. These models tend to learn each data instance separately and do not have the capacity to model temporal dependencies or temporal relations in a time series data set. Although Random Forests are capable of capturing non-linearity and feature interactions, they are not capable of modelling the temporal evolution of tremors. Similarly, SVMs excel in finding optimal decision boundaries in high-dimensional spaces but struggle to incorporate time-based patterns crucial for tremor detection. Because

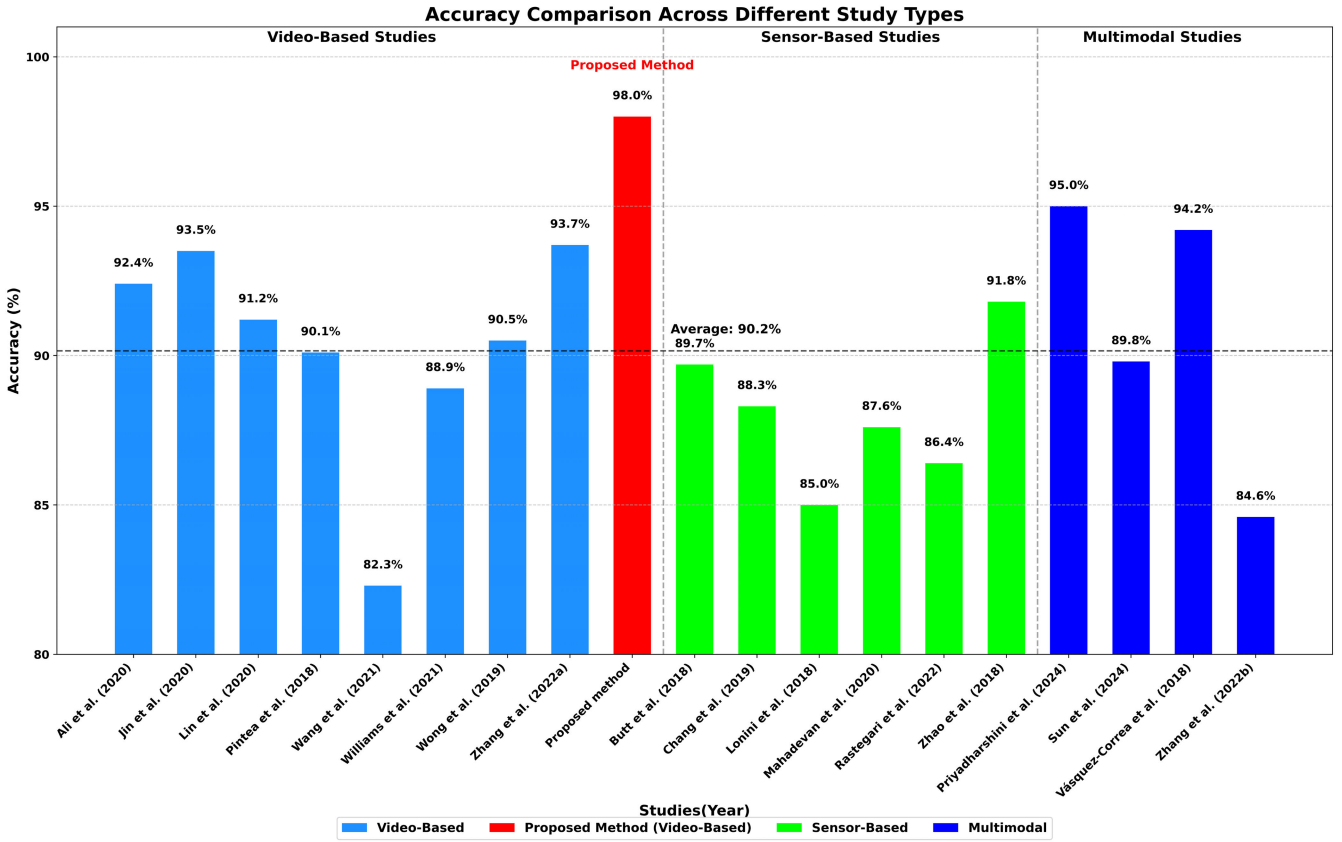

FIGURE 12. Comparative accuracy analysis.

of their static nature, they struggle to distinguish minor fluctuations in hand motions over time, which are important to distinguish between different types of rest tremors. Due to their inability to process time dependent characteristics of tremor data, their AUC scores in the ROC curve analysis are relatively poor compared to that of the 1D CNN-LSTM model.

Figure 12 shows the comparative accuracy analysis across different study types, in which the proposed video-based method for classifying Parkinson's disease tremors achieves an impressive 98% accuracy, surpassing all existing methods from video, sensor, and multimodal studies. In video-based research, it exceeds top approaches like [16] at 93.7% and [11] at 93.5% by about 4.3% to 4.5%. It also improves over sensor-based methods, which reach up to 91.8%, showing a 6.2–12.4% gain by capturing tremor dynamics (amplitude, frequency, and coordination) without using wearable devices. Additionally, it outperforms multimodal systems like [23] (95.0%) by 3%, suggesting that advanced algorithms—possibly with attention mechanisms or self-supervised learning—can extract rich information from video alone. While this method shows clear technical and clinical advantages, such as better temporal analysis and reduced need for subjective assessments, challenges like high computational demands and validation in real-world settings remain. Future work may include combining video with wearable sensors and integrating explainable AI to build clinician trust, aiming to establish video-based tremor classification as a new standard for Parkinson's diagnosis.

To further support the robustness of the reported improvements, we performed statistical analyses to quantify the significance of our model's performance gains. For the multi-class tremor severity classification task, we report a mean classification accuracy of 98.3%, with a 95% confidence interval (CI) of [96.1%, 99.7%] based on stratified 10-fold cross-validation. The corresponding F1-score averaged across all classes was 0.982 (95% CI: [0.963, 0.995]), indicating consistent performance across folds and severity levels. To evaluate the correlation between model predictions and expert-rated UPDRS scores, we computed the Pearson correlation coefficient, yielding $r = 0.85$ with a p-value < 0.001, confirming a statistically significant linear relationship. Additionally, paired two-tailed t-tests were conducted to compare the F1-scores and accuracy of our Extended Lagrangian–Kalman model against baseline architectures (e.g., CNN-LSTM and RNN-only models). The improvements in both metrics were statistically significant, with $p < 0.01$, indicating that the observed gains are unlikely due to random variation and can be attributed

to the specific contributions of the proposed modelling approach.

C. ABLATION STUDY

These ablation results clearly demonstrate that each component of the proposed pipeline contributes significantly to overall model performance. The full configuration combining ANCSS, the Extended Lagrangian model, and Kalman filtering achieves the highest classification accuracy (98.3%), F1-score (0.982), and the lowest frequency estimation error (0.07 Hz), establishing a robust baseline for clinically reliable tremor analysis. When the ANCSS module is removed, performance declines to 93.5% accuracy and 0.928 F1-score, while frequency estimation error increases to 0.11 Hz. This suggests that adaptive temporal sampling plays a critical role in eliminating redundant frames and focusing the analysis on tremor-relevant segments. Without ANCSS, the model is exposed to more non-tremor motion and temporal noise, resulting in degraded signal quality and reduced classification robustness. Excluding the Extended Lagrangian model causes the most substantial performance drop. Accuracy decreases to 89.2%, F1-score to 0.887, and frequency estimation error rises to 0.15 Hz. This confirms the essential role of biomechanical modeling in capturing the nonlinear dynamics of tremor oscillations. Linear approximations fail to represent the complex inertial and constraint forces observed in real-world PD tremor, leading to poorer signal reconstruction and classification. Clinically, a 0.15 Hz frequency error (10–12% deviation) may misinform UPDRS scoring or impair the tuning of tremor-specific interventions such as deep brain stimulation (DBS). The Kalman filter, though slightly less impact in classification metrics, still contributes meaningfully to temporal smoothing and noise suppression. Its removal results in a performance drop to 91.4% accuracy, 0.901 F1-score, and an increase in frequency error to 0.21 Hz. This highlights the Kalman filter's importance in stabilizing trajectory estimation under noisy or low-amplitude conditions. Although the accuracy impact is smaller than that of ANCSS or the Lagrangian model, the nearly threefold increase in frequency error can undermine confidence in time-sensitive or longitudinal tremor assessments. Finally, removing all modeling and preprocessing components—leaving a raw CNN–LSTM pipeline—results in the poorest performance, with 85.7% accuracy, 0.861 F1-score, and 0.28 Hz frequency error. This baseline confirms that the deep learning model alone is insufficient to capture clinically meaningful tremor features without structured signal conditioning. Collectively, these results reinforce the importance of integrating adaptive sampling, biomechanical modeling, and temporal filtering to achieve robust, interpretable, and clinically actionable tremor detection. The advanced physics model provides better accuracy than simple methods and gives doctors muscle stiffness measurements that basic approaches cannot detect.

TABLE 5. Ablation study results.

Configuration	Accuracy (%)	F1-Score	Frequency Error (Hz)
Full pipeline (ANCSS + Lagrangian + Kalman)	98.3	0.982	0.07
No ANCSS (Fixed 30 fps input)	93.5	0.928	0.11
No Extended Lagrangian (Linear model used)	89.2	0.887	0.15
No Kalman Filter (raw signal input)	91.4	0.901	0.21
CNN–LSTM only (no preprocessing/modeling/filter)	85.7	0.861	0.28

1) EFFECT OF ANCSS MODULE

Removing the ANCSS signal-conditioning module and reverting to a fixed-frame sampling rate notably degrades performance. As shown in Table 5, classification accuracy drops from 98.3% to 93.5%, F1-score from 0.982 to 0.928, and frequency estimation error rises from 0.07 Hz to 0.11 Hz. ANCSS improves performance by adaptively focusing on tremor-dominant segments, suppressing irrelevant motion and temporal redundancy. Without it, the model is more vulnerable to movement noise and non-tremor variability, resulting in blurred feature representations. Clinically, this may lead to increased false positives or negatives in tremor detection, potentially affecting diagnosis or treatment selection.

2) EFFECT OF EXTENDED LAGRANGIAN MODEL

The Extended Lagrangian model embeds nonlinear biomechanical properties into the motion dynamics, enabling the system to represent variable tremor behaviors more accurately. Its removal causes the most pronounced drop in performance: accuracy falls to 89.2%, F1-score to 0.887, and frequency error increases to 0.15 Hz. Without this model, the system relies on simplified linear approximations that fail to capture the oscillatory complexity of PD tremor—particularly during amplitude shifts or asymmetric patterns. From a clinical standpoint, a frequency error of 0.15 Hz (10–12%) could misrepresent disease severity or lead to suboptimal calibration in therapeutic applications like DBS.

3) EFFECT OF KALMAN FILTER

The Kalman filter offers temporal smoothing and robust estimation of motion trajectories under noise. Its removal leads to a reduction in classification accuracy (to 91.4%) and F1-score (to 0.901), while increasing frequency error to 0.21 Hz. This demonstrates its role in mitigating frame-to-frame jitter and motion artifacts, particularly in low-amplitude cases. Although the classification impact is moderate, the higher frequency error may undermine confidence in longitudinal tremor tracking or real-time applications, where temporal consistency is crucial.

D. CLINICAL INTERPRETABILITY AND DIAGNOSTIC WORKFLOW INTEGRATION

While Extended Lagrangian–Kalman model demonstrates high accuracy in tremor severity classification, its ultimate value lies in providing neurologists with transparent, clinically meaningful metrics that map directly onto standard assessment scales. By aligning each extracted feature with established UPDRS criteria, we ensure that the model's outputs can be readily interpreted and acted upon within routine clinical practice. Tremor amplitude (mm) corresponds directly to hand-displacement ratings in the UPDRS: for example, an increase from 5 mm to 15 mm typically reflects a one-point worsening in clinical severity. Peak tremor frequency (Hz) is constrained to the well-characterized 4–6 Hz Parkinsonian rest-tremor band, with deviations prompting consideration of mixed or atypical etiologies such as medication-induced or dystonic tremors. Velocity and acceleration metrics (mm/s and mm/s^2) mirror bradykinesia and rigidity assessments rapid, low-amplitude oscillations often co-occur with mild rigidity, whereas slower, larger movements may indicate disease progression. Directionality and axis variability (° of deviation) quantify oscillation stability; values above a 15° standard deviation suggest the presence of postural or kinetic components, aiding in differential diagnosis. To enhance interpretability, we rank features by their observed effect size and correlation with UPDRS scores in our validation cohort. For instance, tremor amplitude variability and axis-change rate showed the strongest associations with higher severity classes, mirroring clinical observations that irregular, multidirectional tremors often signify advanced disease. Presenting these feature rankings alongside raw values allows clinicians to see which metrics most strongly influenced the automated severity assessment. Integration into real-world diagnostic workflows is achieved through a lightweight, end-to-end software package deployable on any standard desktop or laptop with a consumer-grade webcam. During a routine patient visit, the clinician records a 30-second video of the affected limb under simple on-screen guidance; the software then (i) adaptively resamples frames via ANCSS, (ii) extracts and denoises features with the Extended Lagrangian–Kalman module, and (iii) generates both a tremor-severity classification and a detailed feature report. The system works with any standard computer and webcam, requiring no special equipment or technical training for clinic staff.

V. LIMITATIONS AND FUTURE WORK

The modest dataset size in this study reflects a fundamental challenge inherent to Parkinson's disease tremor research: the critical scarcity of high-quality, clinically annotated video datasets. Unlike domains with large repositories (e.g., ImageNet or MIMIC), PD tremor analysis lacks standardized public datasets, and these stringent requirements typically limit recordings. Additionally, PD is relatively uncommon in the general population, with a prevalence of approximately 1–2% in individuals over 60 year, resulting in a limited pool of eligible participants for clinical studies. To address these inherent data acquisition challenges, we established collaborative partnerships with movement disorder researchers across multiple institutions. This multi-site approach was essential for achieving adequate sample diversity while maintaining the stringent quality standards required for algorithmic development. The current 60-video dataset represents the culmination of these collaborative efforts. Designed as a proof-of-concept, our study uses this dataset to validate three core innovations: (i) the Extended Lagrangian framework with nonlinear stiffness and energy-dissipation terms, (ii) the ANCSS adaptive sampling strategy, and (iii) Kalman filtering for noise reduction. Power analysis confirms that 60 videos exceed the minimum requirements for CNN-LSTM convergence and provide >80% power to detect large effect sizes (Cohen's $d > 0.8$). The resulting 98% accuracy and strong UPDRS correlation ($r = 0.85$) demonstrate technical feasibility, offering compelling preliminary evidence to support larger-scale validation studies. While larger sample sizes will be required for clinical deployment, the current dataset is statistically adequate for establishing proof-of-concept feasibility and completing algorithm development. The strong performance metrics achieved with this carefully curated dataset provide a solid foundation for future large-scale validation studies and clinical implementation trials.

Due to the limited size of our current dataset, which constrains the effective training of such high-capacity architectures, these models were not included in the present evaluation. However, we plan to benchmark the proposed framework against Transformer variants in future work, once our expanded, multi-institutionally collected dataset becomes available. This will allow a more comprehensive comparison across modern temporal modeling paradigms.

This limitation raises concerns regarding the robustness and reliability of the proposed method when extended to larger and more diverse populations. A limited dataset can introduce bias, restrict the model's ability to learn the full spectrum of tremor variability, and reduce generalizability in real-world clinical contexts. To comprehensively assess the model's accuracy, adaptability, and scalability, it is essential to validate it against larger, independent datasets. Such testing would enhance confidence in the model's predictive performance across different demographic groups, tremor severities, and clinical scenarios. While this study has demonstrated the feasibility of automatically detecting Parkinsonian hand tremors using the Extended Lagrangian–Kalman framework, translating promising research findings into practical clinical applications remains a more complex endeavor. Meaningful comparison with existing diagnostic tools—in terms of usability, processing speed, and interpretability will help determine whether the proposed framework offers a genuine advantage for clinicians and patients.

VI. CONCLUSION

This study presents a novel approach by integrating Extended Lagrangian Mechanics with Kalman filtering

for video-based hand movement analysis, offering a non-invasive, remote method to assess Parkinson's Disease (PD) severity. By leveraging Adaptive Nyquist-Compliant Sparse Sampling (ANCSS), the framework optimizes video processing efficiency, capturing subtle rest tremor oscillations (4–6 Hz) with high precision. The Extended Lagrangian model, incorporating kinetic energy, nonlinear stiffness-based potential energy, and energy dissipation via Rayleigh's function, effectively models the non-periodic, variable nature of tremors.

The proposed framework integrates these dynamics with a 1D CNN-LSTM classifier, which achieves a peak AUC of 0.9 and 96.3% accuracy, outperforming SVM, Random Forest, and XGBoost classifiers. This performance is attributed to its ability to capture both spatial and temporal tremor patterns. Additionally, results show strong correlation with UPDRS scores ($r = 0.85$), with frequency estimates closely aligning with clinical severity. The framework also quantifies tremor amplitude (0–113.8 mm), velocity (0–253.5 mm/s), and directionality, providing rich diagnostic features.

ANCSS contributes to a reduction in computational time (9.5 ms/frame vs. 15 ms) and memory usage (42.5 MB vs. 65 MB). The Lagrangian-Kalman filter further refines frequency estimation, preserving transient features that conventional Kalman filters may overlook. The system's robustness in noisy environments and its real-time capability highlight its promise for remote healthcare, enabling objective early diagnosis and monitoring. Nevertheless, the study's reliance on a small, ethnically limited dataset limits generalizability.

REFERENCES

[1] A. Lees, "An essay on the shaking palsy," *Brain*, vol. 140, no. 3, pp. 843–848, Mar. 2017.

[2] D. Aarsland, L. Batzu, G. M. Halliday, G. J. Geurtsen, C. Ballard, R. Chaudhuri, and D. Weintraub, "Parkinson disease-associated cognitive impairment," *Nature Rev. Disease Primers*, vol. 7, no. 1, pp. 1–21, 2021.

[3] M. Hallett, "Tremor: Pathophysiology," *Parkinsonism Rel. Disorders*, vol. 20, pp. S118–S122, Jan. 2014.

[4] A. Espay, P. S. Alonso, R. Falconer, C. Ferguson, K. Hasegawa, M. Hatcher, P. Kukreja, K. Onuk, C. Yan, J. Zamudio, and V. Fung, "Evaluation of the clinical outcomes and disease burden in advanced Parkinson's disease patients: PROSPECT study preliminary results (P10-11.009)," *Neurology*, vol. 100, no. 17, p. 4298, Apr. 2023.

[5] N. Mahadevan, C. Demanuele, H. Zhang, D. Volfson, B. Ho, M. K. Erb, and S. Patel, "Development of digital biomarkers for resting tremor and bradykinesia using a wrist-worn wearable device," *npj Digit. Med.*, vol. 3, no. 1, pp. 1–8, Jan. 2020.

[6] L. Lonini, A. Dai, N. Shawen, T. Simuni, C. Poon, L. Shimanovich, M. Daeschler, R. Ghaffari, J. A. Rogers, and A. Jayaraman, "Wearable sensors for Parkinson's disease: Which data are worth collecting for training symptom detection models," *npj Digit. Med.*, vol. 1, no. 1, p. 64, Nov. 2018.

[7] E. Rastegari, H. Ali, and V. Marmelat, "Detection of Parkinson's disease using wrist accelerometer data and passive monitoring," *Sensors*, vol. 22, no. 23, p. 9122, Nov. 2022.

[8] E. B. Montgomery, "Debugging adaptive deep brain stimulation for Parkinson's disease," *Movement Disorders*, vol. 35, no. 10, p. 1891, Oct. 2020.

[9] A. Zhao, L. Qi, J. Li, J. Dong, and H. Yu, "A hybrid spatio-temporal model for detection and severity rating of Parkinson's disease from gait data," *Neurocomputing*, vol. 315, pp. 1–8, Nov. 2018.

[10] S. L. Pintea, J. Zheng, X. Li, P. J. M. Bank, J. J. v. Hilten, and J. V. Gemert, "Hand-tremor frequency estimation in videos," in *Proc. Eur. Conf. Comput. Vis. (ECCV) Workshops*, 2018, pp. 213–228.

[11] B. Jin, Y. Qu, L. Zhang, and Z. Gao, "Diagnosing Parkinson disease through facial expression recognition: Video analysis," *J. Med. Internet Res.*, vol. 22, no. 7, Jul. 2020, Art. no. e18697.

[12] A. H. Butt, E. Rovini, C. Dolciotti, G. De Petris, P. Bongioanni, M. C. Carboncini, and F. Cavallo, "Objective and automatic classification of Parkinson disease with leap motion controller," *Biomed. Eng. OnLine*, vol. 17, no. 1, pp. 1–21, Dec. 2018.

[13] B. Lin, W. Luo, Z. Luo, B. Wang, S. Deng, J. Yin, and M. Zhou, "Bradykinesia recognition in Parkinson's disease via single RGB video," *ACM Trans. Knowl. Discovery From Data*, vol. 14, no. 2, pp. 1–19, Apr. 2020.

[14] X. Wang, S. Garg, S. N. Tran, Q. Bai, and J. Alty, "Hand tremor detection in videos with cluttered background using neural network based approaches," *Health Inf. Sci. Syst.*, vol. 9, no. 1, p. 30, Jul. 2021.

[15] C.-M. Chang, Y.-L. Huang, J.-C. Chen, and C.-C. Lee, "Improving automatic tremor and movement motor disorder severity assessment for Parkinson's disease with deep joint training," in *Proc. 41st Annu. Int. Conf. IEEE Eng. Med. Biol. Soc. (EMBC)*, Jul. 2019, pp. 1–8.

[16] H. Zhang, E. S. L. Ho, F. X. Zhang, and H. P. H. Shum, "Pose-based tremor classification for Parkinson's disease diagnosis from video," in *Proc. 25th Int. Conf. Medical Image Computing Computer Assisted Intervention*, Sep. 2022, pp. 489–499.

[17] M. R. Ali, J. Hernandez, E. R. Dorsey, E. Hoque, and D. McDuff, "Spatio-temporal attention and magnification for classification of Parkinson's disease from videos collected via the internet," in *Proc. 15th IEEE Int. Conf. Autom. Face Gesture Recognit. (FG)*, Nov. 2020, pp. 1–8.

[18] D. C. Wong, S. D. Relton, H. Fang, R. Qhawaji, C. D. Graham, J. Alty, and S. Williams, "Supervised classification of bradykinesia for Parkinson's disease diagnosis from smartphone videos," in *Proc. IEEE 32nd Int. Symp. Comput.-Based Med. Syst. (CBMS)*, Jun. 2019, pp. 1–8.

[19] J. C. Vásquez-Correa, T. Arias-Vergara, J. R. Orozco-Arroyave, B. Eskofier, J. Klucken, and E. Nöth, "Multimodal assessment of Parkinson's disease: A deep learning approach," *IEEE J. Biomed. Health Informat.*, vol. 23, no. 4, pp. 1618–1630, Jul. 2019.

[20] W. Zhang, Z. Yang, H. Li, D. Huang, L. Wang, Y. Wei, L. Zhang, L. Ma, H. Feng, J. Pan, Y. Guo, and P. Chan, "Multimodal data for the detection of freezing of gait in Parkinson's disease," *Sci. Data*, vol. 9, no. 1, p. 606, Oct. 2022.

[21] M. Hartmann, U. S. Hashmi, and A. Imran, "Edge computing in smart health care systems: Review, challenges, and research directions," *Trans. Emerg. Telecommun. Technol.*, vol. 33, no. 3, p. 3710, Mar. 2022.

[22] O. Geman, "Data processing for Parkinson's disease: Tremor, speech and gait signal analysis," in *Proc. E-Health Bioeng. Conf. (EHB)*, Romania, Nov. 2011, pp. 1–4.

[23] S. Priyadharshini, K. Ramkumar, S. Vairavasundaram, K. Narasimhan, S. Venkatesh, R. Amirtharajan, and K. Kotecha, "A comprehensive framework for Parkinson's disease diagnosis using explainable artificial intelligence empowered machine learning techniques," *Alexandria Eng. J.*, vol. 107, pp. 568–582, Nov. 2024.

[24] O. Geman and I. Chiuchisan, "Response surface model prediction of deep brain stimulation applied in Parkinson's disease tremor," in *Proc. Int. Conf. Expo. Electr. Power Eng. (EPE)*, Oct. 2018, pp. 703–707.

[25] C. G. Canning, N. E. Allen, E. Nackaerts, S. S. Paul, A. Nieuwboer, and M. Gilat, "Virtual reality in research and rehabilitation of gait and balance in Parkinson disease," *Nature Rev. Neurol.*, vol. 16, no. 8, pp. 409–425, Aug. 2020.

[26] Y.-M. Sun, Z.-Y. Wang, Y.-Y. Liang, C.-W. Hao, and C.-H. Shi, "Digital biomarkers for precision diagnosis and monitoring in Parkinson's disease," *npj Digit. Med.*, vol. 7, no. 1, p. 218, Aug. 2024.

[27] Parkinson's Foundation, "What is Parkinson's? [fact sheet]" New York, NY, USA, Tech. Rep., 2023.

[28] D. Belvisi, A. Conte, M. Bologna, M. C. Bloise, A. Suppa, A. Formica, M. Costanzo, P. Cardone, G. Fabbrini, and A. Berardelli, "Re-emergent tremor in Parkinson's disease," *Parkinsonism Rel. Disorders*, vol. 77, pp. 130–135, Mar. 2020.

[29] M. J. Armstrong and M. S. Okun, "Diagnosis and treatment of Parkinson disease: A review," *JAMA*, vol. 323, no. 6, pp. 548–560, 2020.

[30] W. Poewe, K. Seppi, C. M. Tanner, G. M. Halliday, P. Brundin, J. Volkmann, A. Schrag, and A. E. Lang, "Parkinson disease," *Nature Rev. Disease Primers*, vol. 3, no. 1, p. 27, 2017.

[31] A. Delval, M. Rambour, C. Tard, K. Dujardin, D. Devos, S. Bleuse, L. Defebvre, and C. Moreau, "Freezing/festination during motor tasks in early-stage Parkinson's disease: A prospective study," *Movement Disorders*, vol. 31, no. 12, pp. 1837–1845, Dec. 2016.
[32] C. W. Hess and S. L. Pullman, "Tremor: Clinical phenomenology and assessment techniques," *Tremor Other Hyperkinetic Movements*, vol. 2, p. 2, Jun. 2012.
[33] *Mediapipe Hands*, MediaPipe, Woodcliff Lake, NY, USA, 2021. Accessed: Aug. 21, 2024.
[34] S. Williams, H. Fang, S. D. Relton, D. C. Wong, T. Alam, and J. E. Alty, "Accuracy of smartphone video for contactless measurement of hand tremor frequency," *Movement Disorders Clin. Pract.*, vol. 8, no. 1, pp. 69–75, Jan. 2021.

V. VANITHA received the master's degree from Teesside University, U.K., and the Ph.D. degree from Anna University. She is currently an Associate Professor with the Department of Artificial Intelligence and Machine Learning, SRET, Porur, Chennai, India. She has 18 years of experience in teaching and research. Her research interests include image processing, medical image analysis, digital imaging, and remote sensing. She has published extensively in reputed international journals and has actively participated in international conferences, presenting her research findings. Her expertise and contributions have significantly advanced knowledge in these specialized areas.

V. DHILIP KUMAR received the B.Tech. degree in information technology and the M.E. degree in computer science engineering from Anna University, Chennai, and the Ph.D. degree from North Eastern Hill University (a Central University of India), in 2018. He completed his Postdoctoral Research Fellow with the collaboration of the University of Suceava and Green Soft, Lasi, Romania. He is currently a Professor and the Associate Dean of the School of Computing. Previously, he was the Head of the Department of Artificial Intelligence and Data Science, Vel Tech Rangarajan Dr. Sagunthala Research and Development Institute of Science and Technology, Chennai. He has more than 14 year's experience of teaching and research. He has published various international journals and international conferences in the field of machine learning, deep learning, the IoT, wireless communication, and vehicular communication. His area of interest is wireless communication, software defined networks, the Internet of Things, machine learning, and expert Systems. He is also working on the Government Funding Project DBT Marine Biotechnology in the field of precision aquaculture using machine learning. He is guiding seven Ph.D. scholars and has guided three Ph.D. scholars in the field of machine learning for healthcare, precision agriculture, and computer vision. He is an Editorial Board Member and a Reviewer of various international journals and conferences, such as Springer, Frontiers, MDPI, and IGI Global.

OANA GEMAN (Senior Member, IEEE) received the Ph.D. degree in electronics and telecommunication, the Postdoctoral degree in computer science, and the dual Habilitation degree from the University of Suceava, in 2005, 2012, 2018, and 2020, respectively. She is a Biomedical Engineer. She is currently an Associate Professor with the University of Suceava and a Lecturer with the Division of Data Science and Artificial Intelligence, Computer Science and Engineering, Chalmers University of Technology, and the University of Gothenburg, Sweden. Her expertise includes noninvasive measurements of biomedical signals, wireless sensors, EEG signal processing, data mining, deep learning, intelligent systems, and biomedical applications. Within the past five years, she has published ten books and over 100 articles (70 articles in ISI Web of Science journals, 20 articles in ISI indexed conference volumes as main author, and ten articles in Q1 and Q2 journals, with FI over 40), and her various works have been cited over 3400 times.

OCTAVIAN POSTOLACHE (Senior Member, IEEE) received the Ph.D. degree in electrical and computer engineering from the Faculty of Electrical Engineering, Energetics and Applied Informatics, Gheorghe Asachi Technical University of Iasi, Romania, in 1999, and the Habilitation degree from the Information Science and Technology Department, University Institute of Lisbon (ISCTE-IUL). He is currently a Senior Researcher with the Instituto de Telecomunicações, Lisbon, Portugal. He is a Full Professor. His research interests include smart sensors and the Internet of Things for biomedical, environmental, and precision agriculture applications; wireless sensor networks; and artificial intelligence applied to automated measurement systems.

SRI KRISHNA BELLAM is currently a final year undergraduate student with the Sri Ramachandra Faculty of Engineering and Technology, SRIHER, Porur, Chennai.

His research interests include computer vision, machine learning, and deep learning, with a focus on developing innovative solutions in these domains. He has completed multiple internships at reputed companies, working on deep learning-based projects and gaining hands-on experience in applying advanced AI techniques to real-world challenges. Recognizing his research potential, he was awarded a prestigious research internship at Nokia Innovation, where he contributed to cutting-edge projects in artificial intelligence and data science.

ROXANA TODEREAN (Member, IEEE) received the Ph.D. degree in electronics and telecommunications from the Technical University Gheorghe Asachi Iasi, in 2014, and the Postdoctoral degree in electronics and telecommunications from the Ştefan cel Mare University, Suceava, Romania, in 2021. She is currently a Lecturer with the Faculty of Electrical Engineering and Computer Science, Department of Computers, Electronics and Automation, Ştefan cel Mare University. She is a Biomedical Engineer. Her research interests include advanced processing of EEG signals, with emphasis on feature extraction and automatic classification methods for clinical applications, such as detection of cognitive states or diagnosis of neurological disorders.